Composite Structures 132 (2015) 737–745

Contents lists available at ScienceDirect

Composite Structures

journal homepage: www.elsevier.com/locate/compstruct

Two-dimensional dynamic model for composite laminates with embedded magnetostrictive materials

S. Santapuri [b], J.J. Scheidler [a], M.J. Dapino [a,*]

[a] Department of Mechanical and Aerospace Engineering, The Ohio State University, Columbus, OH 43210, USA
[b] Department of Mechanical Engineering, Polytechnic University of Puerto Rico, San Juan 00918, Puerto Rico

ARTICLE INFO

Article history:
Available online 14 May 2015

Keywords:
Magnetostrictive materials
Smart composites
2-D plate theories
Nonlinear modeling
Bending actuators

ABSTRACT

A nonlinear, two-dimensional plate model is presented that describes the dynamic response of composite laminate structures with embedded magnetostrictive materials. The model consists of Navier's equation coupled with a discrete energy-averaged constitutive model for magnetostrictive materials. Assuming a thin composite geometry, the complete three-dimensional model is reduced to a two-dimensional equivalent single layer plate model by assuming a functional form for displacements. The resulting two-dimensional variational form, solved using finite element software, is applied to analyze the displacements of a Galfenol–aluminum composite actuator, wherein Galfenol sheets are embedded into an aluminum substrate. The model is validated at lower frequencies using time domain measurements of the dynamic actuation response of the actuator. This framework is subsequently utilized to perform a parametric study to maximize the tip displacements by varying the geometric parameters: Galfenol location, thickness ratio, and substrate properties. The general finite element framework presented in this paper is applicable to a wider range of magnetostrictive materials and complex composite geometries.
© 2015 Elsevier Ltd. All rights reserved.

1. Introduction

Magnetostrictive materials exhibit the Joule effect, a shape change in response to externally applied magnetic fields, and the Villari effect, a change in magnetic susceptibility of the material when subjected to external stress [1]. These properties make magnetostrictive materials useful in sensing and actuation applications such as active vibration control, energy harvesting, stress and torque sensing, and machining [2,3]. Terfenol-D ($Tb_{0.3}Dy_{0.7}Fe_{1.9}$) exhibits the largest known room-temperature magnetostriction of about 1600 ppm [4], but needs to be operated in compression due to its brittleness. This limitation can be overcome, at the expense of magnetostriction, by embedding Terfenol-D particles in epoxy, polymer, or metal matrices. Galfenol ($Fe_{81.6}Ga_{18.4}$) is a recent magnetostrictive material that exhibits moderate magnetostriction (≈350 ppm), but has structural properties comparable to low-carbon steels, allowing its use in mechanically-harsh environments [2]. Galfenol can be integrated with passive components through fusion welding, machining, or other traditional processes to design multifunctional, load-bearing structures.

Magnetostrictive materials have been used to build active composite structures (consisting of active magnetostrictive and passive metallic components) for a variety of applications. Some examples include a strain sensor [5], torque sensor [6], bioMEMS sensor [7], and a MEMS actuator [8]. The recent development of ultrasonic additive manufacturing (UAM), a solid-state welding process that additively welds thin metal tapes to create complex, metallic composites without melting the parent materials, has the potential to revolutionize this field. It enables the manufacture of complex, 3-D composite geometries that can be composed of internal channels, dissimilar metals, electronics, heat-wicking materials, or smart materials [9–11].

To permit the design, optimization, and control of these advanced composites, transducer models need to be developed in parallel with advancements in the manufacturing technology. A key challenge in developing mathematical models for magnetostrictive materials is their highly nonlinear, anisotropic constitutive behavior. Thus, a transducer model for magnetostrictive composites should be formulated such that it can predict the complex, dynamic response of magnetostrictive materials while accommodating the sophisticated geometries made possible by new manufacturing capabilities.

In the past, composites with thin geometries were modeled using equivalent single layer (ESL) theories that were derived from

* Corresponding author.
E-mail addresses: ssantapuri@pupr.edu (S. Santapuri), scheidler.8@osu.edu (J.J. Scheidler), dapino.1@osu.edu (M.J. Dapino).

http://dx.doi.org/10.1016/j.compstruct.2015.04.062
0263-8223/© 2015 Elsevier Ltd. All rights reserved.

3-D continuum theories by making suitable assumptions about the kinematics of deformation through the thickness of the laminate [12]. These theories allowed the reduction of a 3-D problem to a 2-D problem by assuming a functional form for displacement fields [13]. Early developments of classical plate theories for materials exhibiting coupled behavior were limited by linear constitutive models (e.g., piezoelectric, piezomagnetic). One of the earliest developments includes Mindlin's first-order plate theory for high frequency piezoelectric crystals [12]. Reddy enhanced these models by using a third-order plate theory for thick laminated composites with integrated sensors and actuators [14]. These linear models, although sufficient for some regimes of coupled behavior, are often insufficient to model the nonlinear constitutive response of magnetostrictive materials.

One of the earlier attempts to model magnetostrictive materials with nonlinear constitutive behavior was developed by Kannan and Dasgupta [15]. This paper presented a two-dimensional, quasi-static, finite-element scheme to model the nonlinear interactions between mechanical and magnetic fields in Terfenol-D. Datta et al. [16,17] used classical laminated plate theory with the Armstrong magnetomechanical model to characterize laminated sensors and actuators in the absence of current-induced magnetic fields. Neither of these models accounted for dynamic behavior. More recently, Shu et al. [18] utilized a nonlinear, discrete energy-averaged (DEA) model [19] to simulate the 1-D dynamic response of Galfenol-driven unimorph actuators.

In this work, we present the development of a dynamic, two-dimensional plate model describing the nonlinear magnetomechanical behavior of composite plates containing embedded magnetostrictive materials. The modeling approach is based upon variational principles and the finite element method. Starting from a coupled 3-D formulation, the problem is reduced to a 2-D ESL theory. To model the nonlinear, anisotropic behavior of magnetostrictive materials, an anhysteretic, DEA model developed by Evans and Dapino [19] is utilized. The model is then validated using measurements of the dynamic, bending actuation response of a Galfenol–aluminum composite plate (manufactured using UAM). To illustrate its usefulness for design, the model is applied to a prototype bending actuator composed of an aluminum plate with embedded Galfenol sheets.

The paper is structured as follows: Section 2 presents a 3-D description of a smart composite plate. In Section 3 the 2-D model is developed for thin composite plates starting from the complete 3-D formulation. Section 3.2 summarizes the DEA model developed by Evans and Dapino [19] for fully-coupled magnetostrictive materials with cubic symmetry. The framework outlined in Sections 2 and 3 is applied to a Galfenol–aluminum plate in Section 3.4 and experimentally validated in Section 4. In Section 5, the framework is utilized to perform a parametric study of key geometric parameters to optimize the plate's tip displacement. Finally, the results and contributions of this work are discussed in Section 6.

2. 3-D magnetomechanical model for active composites with embedded magnetostrictive layers

This work considers an active composite plate composed of a metal matrix and embedded magnetostrictive laminae of arbitrary geometry. Fig. 1 shows a schematic of an example composite plate containing embedded magnetostrictive layers.

A 3-D model of the composite plate can be formulated by coupling Navier's equation with a nonlinear constitutive law for the magnetostrictive material and linear Hooke's law for the passive material. In the 3-D weak form, Navier's equation can be written as

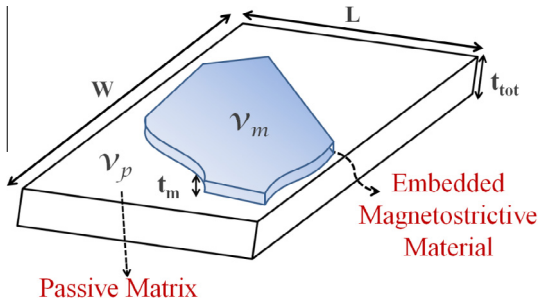

Fig. 1. Schematic of an active composite plate consisting of an embedded magnetostrictive layer of volume $\mathcal{V}_m$ and a passive metallic layer of volume $\mathcal{V}_p$.

$$\int_{V_{tot}} \left[\rho \frac{\partial^2 \mathbf{u}}{\partial t^2} \cdot \delta \mathbf{u} + c \frac{\partial \mathbf{u}}{\partial t} \cdot \delta \mathbf{u} + \mathbf{T} \cdot \delta \mathbf{S} \right] dV = \int_{\partial V_{tot}} \mathbf{t} \cdot \delta \mathbf{u} \, d\partial V + \int_{V_{tot}} \mathbf{f}_B \cdot \delta \mathbf{u} \, dV, \tag{1}$$

where ρ is the density, c represents the viscous damping factor, and $\mathbf{T}$ and $\mathbf{f}_B$ denote, respectively, the stress tensor and external body force acting on the domain V_{tot}. The traction vector $\mathbf{t}$ acts on the boundary ∂V_{tot}. Also, $\mathbf{S}$ and $\mathbf{u}$ represent the strain tensor and displacements at each point in the domain V_{tot}. The strain is defined in terms of the displacements as

$$\mathbf{S} = \frac{1}{2}(\nabla \mathbf{u} + \nabla \mathbf{u}^{\mathrm{T}}), \tag{2}$$

where T denotes the transpose operator. The constitutive equations in the passive and magnetostrictive material domains, respectively, are

$$\mathbf{T} = \mathbf{C} \cdot \mathbf{S} \quad \text{(Passive material)} \tag{3}$$

and

$$\mathbf{T} = \mathbf{T}_m(\mathbf{S}, \mathbf{H}) \qquad \text{(Magnetostrictive material)}, \tag{4}$$

where $\mathbf{C}$ is the stiffness matrix, $\mathbf{H}$ is the magnetic field, and the function $\mathbf{T}_m(\mathbf{S}, \mathbf{H})$ represents the nonlinear constitutive relationship for magnetostrictive materials. In this paper, $\mathbf{T}_m(\mathbf{S}, \mathbf{H})$ is a DEA model developed by Evans and Dapino [19], which will be summarized in Section 3.2. It is assumed that the magnetic field (induced by a conductive coil) is uniform inside the magnetostrictive material and can be approximated using Ampére's Law $H = nI$, where n is the coil constant and I is the current in the coil. By assuming a current-field relationship, the mechanical response of the composite plate can be modeled without considering magnetic circuit equations. This is a good approximation of the field inside a long coil that is tightly wound around a material with a high magnetic permeability, where coil fringing effects can be neglected.

3. Dimensional reduction using classical plate theory

For the analysis of thin composite plates, the conventional modeling approach is based on ESL theories, which are derived from 3-D continuum theories by making suitable assumptions on the kinematics of deformation or the stress state through the thickness of the laminate. These theories allow the reduction of a 3-D problem to a 2-D problem [20].

An ESL plate theory for active composite structures that contain embedded magnetostrictive materials is developed by assuming the following expansion for the displacement field $\mathbf{u}$:

$$\mathbf{u}(x, y, z) = [u, v, w]^{\mathrm{T}} = \sum_{n=0}^{n=\infty} z^n \mathbf{u}^{(n)}(x, y). \tag{5}$$

The simplest form of laminated plate theory is the classical plate theory, where the displacement field takes the form:

$$u(x,y,z,t) = u_0(x,y,t) + z\phi_x(x,y,t), \tag{6}$$
$$v(x,y,z,t) = v_0(x,y,t) + z\phi_y(x,y,t), \tag{7}$$
$$w(x,y,z,t) = w_0(x,y,t), \tag{8}$$

where ϕ_x and ϕ_y denote rotations about the y and x axes, respectively. Assuming that the deformation has only bending and in-plane stretching components (i.e., transverse normal and transverse shear effects are negligible), these rotations are represented as

$$\phi_x = -\frac{\partial w_o}{\partial x}, \quad \phi_y = -\frac{\partial w_o}{\partial y}. \tag{9}$$

Classical plate theories work well for thin composite plates with thickness ratio (ratio of thickness to length or width) less than 0.1. As the thickness increases, higher order theories need to be considered [20]. The displacement forms described in (6)–(9) allow us to ignore the strain components S_{zz}, S_{xz}, and S_{yz}, i.e., the problem reduces to a plane strain problem. The remaining strain components can be written as

$$\begin{bmatrix} S_{xx} \\ S_{yy} \\ S_{xy} \end{bmatrix} = \begin{bmatrix} S^{(0)}_{xx} \\ S^{(0)}_{yy} \\ S^{(0)}_{xy} \end{bmatrix} + z \begin{bmatrix} S^{(1)}_{xx} \\ S^{(1)}_{yy} \\ S^{(1)}_{xy} \end{bmatrix}, \tag{10}$$

where

$$\begin{aligned} S^{(0)}_{xx} &= \frac{\partial u_0}{\partial x}, \quad S^{(0)}_{yy} = \frac{\partial v_0}{\partial y}, \quad S^{(0)}_{xy} = \frac{1}{2}\left(\frac{\partial u_0}{\partial y} + \frac{\partial v_0}{\partial x}\right), \\ S^{(1)}_{xx} &= \frac{\partial \phi_x}{\partial x}, \quad S^{(1)}_{yy} = \frac{\partial \phi_y}{\partial y}, \quad S^{(1)}_{xy} = \frac{1}{2}\left(\frac{\partial \phi_x}{\partial y} + \frac{\partial \phi_y}{\partial x}\right). \end{aligned} \tag{11}$$

To define the stresses in the passive and active subdomains, constitutive equations for each subdomain must be defined.

3.1. Stress components: incorporation of constitutive equations

The composite plate is split into passive and active (magnetostrictive) subdomains, represented by subscripts p and m, respectively.

3.1.1. Passive subdomain constitutive equations

For the passive layers, linear Hooke's law is used, which assumes linear isotropic behavior.[1] The corresponding constitutive equations are

$$\begin{bmatrix} T_{xx} \\ T_{yy} \\ T_{xy} \end{bmatrix}^{(p)} = \frac{E_p}{(1+\nu_p)(1-2\nu_p)} \begin{bmatrix} 1-\nu_p & \nu_p & 0 \\ \nu_p & 1-\nu_p & 0 \\ 0 & 0 & 1-2\nu_p \end{bmatrix} \begin{bmatrix} S_{xx} \\ S_{yy} \\ S_{xy} \end{bmatrix}^{(p)}. \tag{12}$$

The following material parameters are used for the aluminum matrix: Young's modulus $E_p = 69$ GPa, Poisson's ratio $\nu_p = 0.33$, and density $\rho_p = 2700$ kg/m^3.

3.1.2. Magnetostrictive subdomain constitutive equations

The inputs for the magnetostrictive constitutive model are magnetic field and stress, and the outputs are magnetization and strain, which includes magnetoelastic and purely mechanical components. Consequently, the stress–strain constitutive law can be written as

$$\begin{aligned} \begin{bmatrix} T_{xx} \\ T_{yy} \\ T_{xy} \end{bmatrix}^{(m)} &= \frac{E_m}{(1+\nu_m)(1-2\nu_m)} \begin{bmatrix} 1-\nu_m & \nu_m & 0 \\ \nu_m & 1-\nu_m & 0 \\ 0 & 0 & 1-2\nu_m \end{bmatrix} \\ &\times \left\{ \begin{bmatrix} S_{xx} \\ S_{yy} \\ S_{xy} \end{bmatrix}^{(m)} - \boldsymbol{\lambda}\left(\mathbf{T}^{(m)}, \mathbf{H}\right) \right\}, \end{aligned} \tag{13}$$

where $\boldsymbol{\lambda}$ denotes the macroscopic magnetoelastic strain (magnetostriction) in the magnetostrictive material. Due to the dependence of $\boldsymbol{\lambda}$ on $\mathbf{T}^{(m)}$, (13) is implicit and must be calculated by inverting the constitutive model of the magnetostrictive material after solving for the total strain. This work utilizes a fully-coupled, nonlinear DEA model for cubic magnetostrictive materials developed by Evans and Dapino [19], which is accurate yet efficient and has been successfully used for the modeling of Galfenol-based systems [21,18,22,23]. This model is summarized in the following section. To model composite structures containing Terfenol-D constituents, the analogous DEA model for Terfenol-D developed by Chakrabarti and Dapino [24] can be used instead, with minor changes to the proposed framework.

3.2. Review of the two-dimensional discrete energy-averaged model for cubic magnetostrictive materials

The energy-averaged class of models calculates the macroscopic constitutive response as an energy-weighted summation of the response due to domains aligned along different crystallographic directions. With homogeneously-distributed, fixed orientations (as in Armstrong's model [25]), obtaining high accuracy requires a large number of possible orientations, which results in significant computational effort.

To improve the computational efficiency while preserving accuracy, Evans and Dapino [19] restricted the number of possible orientations to six by considering only the directions that minimize an energy functional that is locally-defined around each of the six easy crystallographic directions. The total free energy $\overset{k}{G}$ of a magnetic moment oriented in the vicinity of the kth easy direction $\overset{k}{\mathbf{c}}$ is formulated as the sum of the local magnetocrystalline (anisotropy),[2] magnetoelastic (magnetomechanical coupling) and magnetic field (Zeeman) energies. This energy can be written in matrix form as

$$\overset{k}{G} = \frac{1}{2}\,\overset{k}{\mathbf{m}}\cdot\mathbf{K}\,\overset{k}{\mathbf{m}} - \overset{k}{\mathbf{m}}\cdot\overset{k}{\mathbf{B}} + \overset{k}{K}_0 \quad (k = 1,2,\ldots,6) \tag{14}$$

where $\overset{k}{\mathbf{m}}$ is the magnetic moment direction,

$$\mathbf{K} = \begin{bmatrix} K - 3\lambda_{100}T_{xx} & -3\lambda_{111}T_{xy} & 0 \\ -3\lambda_{111}T_{xy} & K - 3\lambda_{100}T_{yy} & 0 \\ 0 & 0 & K \end{bmatrix}, \tag{15}$$

$$\overset{k}{\mathbf{B}} = \begin{bmatrix} \overset{k}{c}_1 K + \mu_o M_s H_1 & \overset{k}{c}_2 K + \mu_o M_s H_2 & \overset{k}{c}_3 K \end{bmatrix}^{\mathrm{T}}, \tag{16}$$

where K and $\overset{k}{K}_0$ are anisotropy energy constants, M_s is the saturation magnetization, λ_{100} and λ_{111} are magnetostriction constants, and μ_o is the permeability of free space. The minimization of (14) is constrained ($\|\overset{k}{\mathbf{m}}\| = 1$) and solved, through the use of Lagrange multipliers, as an inhomogeneous eigenvalue problem [19]. By approximating the constraint using $\|\overset{k}{\mathbf{m}}\| \approx \overset{k}{\mathbf{m}}\cdot\overset{k}{\mathbf{c}}$, the minimization problem has the explicit solution

[1] This assumption is valid for the aluminum matrix considered in this paper. However, anisotropic materials can be easily considered by using a stiffness matrix with fewer restrictions on material symmetry.

[2] The improved anisotropy energy given by Chakrabarti [26] is used.

$$\overset{k}{\mathbf{m}} = \mathbf{K}^{-1}\left[\overset{k}{\mathbf{B}} + \frac{1 - \overset{k}{\mathbf{c}}\cdot\mathbf{K}^{-1}\overset{k}{\mathbf{B}}}{\overset{k}{\mathbf{c}}\cdot\mathbf{K}^{-1}\overset{k}{\mathbf{c}}}\overset{k}{\mathbf{c}}\right]. \tag{17}$$

The anhysteretic volume fraction $\overset{k}{\xi}_{an}$ of magnetic domains oriented along the kth minimum energy direction is calculated using Boltzmann-type averaging,

$$\overset{k}{\xi}_{an} = \frac{\exp\left(-\overset{k}{G}/\Omega\right)}{\sum_{j=1}^{r}\exp\left(-\overset{j}{G}/\Omega\right)}, \tag{18}$$

where Ω is a smoothing constant. Macroscopic anhysteretic material behavior is obtained by summing the contributions due to each minimum energy magnetization direction $\overset{k}{\mathbf{m}}$ weighted by their corresponding volume fraction. Thus, the strain tensor $\mathbf{S}$ is given by the sum of the elastic and magnetoelastic strains,

$$\mathbf{S} = \mathbf{s}\mathbf{T} + \boldsymbol{\lambda} = \mathbf{s}\mathbf{T} + \sum_{k=1}^{r}\overset{k}{\xi}_{an}\overset{k}{\bar{\boldsymbol{\lambda}}}, \tag{19}$$

where $\mathbf{s}$ is the 3×3 compliance tensor for Galfenol and $\overset{k}{\bar{\boldsymbol{\lambda}}}$ represents the magnetostriction of a ferromagnetic material with cubic symmetry due to the kth minimum energy direction,

$$\overset{k}{\bar{\boldsymbol{\lambda}}} = \begin{bmatrix} 3/2\lambda_{100}\overset{k}{m}_1{}^2 \\ 3/2\lambda_{100}\overset{k}{m}_2{}^2 \\ 3\lambda_{111}\ \overset{k}{m}_1\ \overset{k}{m}_2 \end{bmatrix}. \tag{20}$$

Material constants for Galfenol used in this model are[3]: $E_m = 57$ GPa, $\nu_m = 0.3$, $\rho_m = 7870$ kg/m^3, $K = 27.1$ kJ/m^3, $K_0 = 0.021$ kJ/m^3, $\mu_0 M_s = 1.3$ T, $\lambda_{100} = 156.56$ ppm, $\lambda_{111} = 1/3\times(-20)$ ppm, and $\Omega = 1300$ J/m^3.

As detailed in Section 3.1, to integrate the constitutive Eq. (19) into Navier's equation (1), inversion of the constitutive model is required, wherein stress is the output (dependent variable) and strain is the input (independent variable). Owing to the nonlinear dependence of $\mathbf{S}$ on $\mathbf{T}$ and $\mathbf{H}$ and the homogenization equation (18), an analytical inverse does not exist. Following the approach of Chakrabarti and Dapino [21], the inversion is performed using the quasi-Newton SR1 formula. By also utilizing the Sherman-Morrison formula, the need for calculating and inverting the material Jacobian within the iteration loop is avoided. The use of an iterative inversion algorithm adds computational cost, but allows the solution procedure to retain the full nonlinearity of the constitutive model, unlike inversions based upon linearization of the constitutive model. Having presented the constitutive model for the passive and active subdomains, we now proceed to derive the 2-D ESL plate theory for the magnetostrictive composite plate.

3.3. Derivation of equivalent two-dimensional variational principle

To derive the 2-D weak form starting from the 3-D composite plate model (1), the 3-D weak form is recalled,

$$\int_{V_{tot}}\left[\rho\frac{\partial^2\mathbf{u}}{\partial t^2}\cdot\delta\mathbf{u} + c\frac{\partial\mathbf{u}}{\partial t}\cdot\delta\mathbf{u} + \mathbf{T}\cdot\delta\mathbf{S}\right]dV - \int_{\partial V_{tot}}\mathbf{t}\cdot\delta\mathbf{u}\,d\partial V - \int_{V_{tot}}\mathbf{f}_B\cdot\delta\mathbf{u}\,dV = 0. \tag{21}$$

[3] The Galfenol material parameters (including damping coefficient) used in this framework are optimized for a 2-D problem to accommodate for the plane strain assumption.

The variational form of 2-D plate theory is derived by substituting stress, displacement, and strain expressions (6)–(13) into the 3-D formulation of Navier's equation (21), which decouples the through-thickness integration from the in-plane integration. With Ω_e as the ESL area and t_{tot} as the plate's thickness, the first term on the left-hand side of (21) is reduced to 2-D as follows:

$$\begin{aligned}\int_{V_{tot}}\rho\frac{\partial^2\mathbf{u}}{\partial t^2}\cdot\delta\mathbf{u}dV &= \int_{t_{tot}}\int_{\Omega_e}\left[\rho\frac{\partial^2 u}{\partial t^2}\delta u + \rho\frac{\partial^2 v}{\partial t^2}\delta v + \rho\frac{\partial^2 w}{\partial t^2}\delta w\right]dxdydz \\ &= \int_{\Omega_e}\left\{\left(\int_{t_{tot}}\rho dz\right)\frac{\partial^2 u_o}{\partial t^2}\delta u_o + \left(\int_{t_{tot}}\rho z dz\right)\frac{\partial^2\phi_x}{\partial t^2}\delta u_o \right. \\ &\quad + \left(\int_{t_{tot}}\rho z dz\right)\frac{\partial^2 u_o}{\partial t^2}\delta\phi_x + \left(\int_{t_{tot}}\rho z^2 dz\right)\frac{\partial^2\phi_x}{\partial t^2}\delta\phi_x \\ &\quad + \left(\int_{t_{tot}}\rho dz\right)\frac{\partial^2 v_o}{\partial t^2}\delta v_o + \left(\int_{t_{tot}}\rho z dz\right)\frac{\partial^2\phi_y}{\partial t^2}\delta v_o \\ &\quad + \left(\int_{t_{tot}}\rho z dz\right)\frac{\partial^2 v_o}{\partial t^2}\delta\phi_y + \left(\int_{t_{tot}}\rho z^2 dz\right)\frac{\partial^2\phi_y}{\partial t^2}\delta\phi_y \\ &\quad \left. + \left(\int_{t_{tot}}\rho dz\right)\frac{\partial^2 w_o}{\partial t^2}\delta w_o\right\}dxdy.\end{aligned} \tag{22}$$

The remaining terms in (21) are reduced to 2-D in a similar manner. The density integrals in (22) depend only on the geometry and constituent materials and must be evaluated only once. Similar integrals will arise for the viscous damping factor c and the stress terms T_{xx}, T_{xy}, and T_{yy}. In the interest of simplifying the presentation of equations, the following equivalent properties for the 2-D plate are defined:

$$\bar{\rho}_k = \int_{t_{tot}}\rho z^k dz, \quad \bar{c}_k = \int_{t_{tot}} c z^k dz \quad (k = 0,1,2) \tag{23}$$

$$\begin{Bmatrix} N_{xx} \\ N_{yy} \\ N_{xy}\end{Bmatrix} = \int_{t_{tot}}\begin{Bmatrix} T_{xx} \\ T_{yy} \\ T_{xy}\end{Bmatrix}dz, \quad \begin{Bmatrix} M_{xx} \\ M_{yy} \\ M_{xy}\end{Bmatrix} = \int_{t_{tot}}\begin{Bmatrix} T_{xx} \\ T_{yy} \\ T_{xy}\end{Bmatrix}z dz. \tag{24}$$

Using these representations, the weak form of the equations reduce to

$$\begin{aligned}\int_\tau\left\{\int_{\Omega_e}\left[\bar{\rho}_o\left(\frac{\partial^2 u_o}{\partial t^2}\delta u_o + \frac{\partial^2 v_o}{\partial t^2}\delta v_o + \frac{\partial^2 w_o}{\partial t^2}\delta w_o\right)\right.\right. \\ + \bar{c}_o\left(\frac{\partial u_o}{\partial t}\delta u_o + \frac{\partial v_o}{\partial t}\delta v_o + \frac{\partial w_o}{\partial t}\delta w_o\right) \\ + \bar{\rho}_1\left(\frac{\partial^2\phi_x}{\partial t^2}\delta u_o + \frac{\partial^2\phi_y}{\partial t^2}\delta v_o + \frac{\partial^2 u_o}{\partial t^2}\delta\phi_x + \frac{\partial^2 v_o}{\partial t^2}\delta\phi_y\right) \\ + \bar{c}_1\left(\frac{\partial\phi_x}{\partial t}\delta u_o + \frac{\partial\phi_y}{\partial t}\delta v_o + \frac{\partial u_o}{\partial t}\delta\phi_x + \frac{\partial v_o}{\partial t}\delta\phi_y\right) \\ + \bar{\rho}_2\left(\frac{\partial^2\phi_x}{\partial t^2}\delta\phi_x + \frac{\partial^2\phi_y}{\partial t^2}\delta\phi_y\right) + \bar{c}_2\left(\frac{\partial\phi_x}{\partial t}\delta\phi_x + \frac{\partial\phi_y}{\partial t}\delta\phi_y\right) \\ \left. + N_{xx}\delta S_{xx}^{(0)} + N_{xy}\delta S_{xy}^{(0)} + N_{yy}\delta S_{yy}^{(0)} + M_{xx}\delta S_{xx}^{(1)} + M_{xy}\delta S_{xy}^{(1)} + M_{yy}\delta S_{yy}^{(1)}\right]dxdy \\ \left. - \int_{\partial\Omega_e}\left(\hat{N}_{nn}\delta u_{on} + \hat{N}_{ns}\delta u_{os} - \hat{M}_{nn}\frac{\partial\delta w_o}{\partial n} - \hat{M}_{ns}\frac{\partial\delta w_o}{\partial s} + \hat{Q}_n\delta w_o\right)ds\right\}dt = 0,\end{aligned} \tag{25}$$

where $\partial\Omega_e$ represents the boundary to Ω_e and τ represents the time over which the dynamic system is studied. Also, the boundary terms $\hat{N}_{nn}$, $\hat{N}_{ns}$, $\hat{M}_{nn}$, $\hat{M}_{ns}$, and $\hat{Q}_n$ are defined as

$$\begin{Bmatrix}\hat{N}_{nn} \\ \hat{N}_{ns}\end{Bmatrix} = \int_{t_{tot}}\begin{Bmatrix}\hat{\sigma}_{nn} \\ \hat{\sigma}_{ns}\end{Bmatrix}dz, \quad \begin{Bmatrix}\hat{M}_{nn} \\ \hat{M}_{ns}\end{Bmatrix} = \int_{t_{tot}}\begin{Bmatrix}\hat{\sigma}_{nn} \\ \hat{\sigma}_{ns}\end{Bmatrix}z dz, \quad \hat{Q}_n = \int_{t_{tot}}\hat{\sigma}_{nz}dz, \tag{26}$$

where $\hat{\sigma}_{nn}$, $\hat{\sigma}_{ns}$, and $\hat{\sigma}_{nz}$ are the specified stress components on the portion of the boundary $\partial\Omega_e$. Through additional knowledge of the

composite geometry and the constituent material properties, the integrals listed in (23) and (24) can be evaluated. These expressions, when substituted into the weak form (25), will provide the complete system model in 2-D.

The model presented above is general and applies to thin composite plates of arbitrary construction that contain magnetostrictive materials. In what follows, we specialize this 2-D variational form to a composite plate actuator consisting of a Galfenol layer embedded into an aluminum matrix.

3.4. 2-D variational form

To develop the equivalent 2-D system corresponding to the 3-D composite plate described in Fig. 1, the integral terms that appear in the 2-D variational form (25) are evaluated. For this application, it is assumed that the plate is only excited by an external magnetic field (i.e., there are no external forces and the integrals in Eq. (26) equate to zero). This excitation enters the model through the magnetostriction of the Galfenol sheets, which loads and deforms the passive volume. The electromagnetic body forces and rotary inertia terms are also ignored. This translates to ignoring the dynamic terms with coefficients $\bar{\rho}_1$, $\bar{\rho}_2$, $\bar{c}_1$, and $\bar{c}_2$.

The plate is divided into two equivalent 2-D subdomains (Fig. 2), i.e., (i) the passive subdomain $\mathcal{A}_p$ and (ii) the active subdomain $\mathcal{A}_m$. The integrals (23) and (24), which are evaluated using the composite's dimensions and its material properties, are substituted into (25) to deduce the 2-D variational form. The density integrals can be calculated as

$$\begin{aligned}
&\textbf{Passive } \mathcal{A}_p : \bar{\rho}_k = \int_{t_{tot}} \rho z^k \, dz = \frac{\rho_p}{k+1}\left(z_1^{k+1} - z_4^{k+1}\right), \\
&\textbf{Active } \mathcal{A}_m : \bar{\rho}_k = \frac{\rho_p}{k+1}\left(z_1^{k+1} - z_2^{k+1}\right) + \frac{\rho_m}{k+1}\left(z_2^{k+1} - z_3^{k+1}\right) \\
&\qquad\qquad + \frac{\rho_p}{k+1}\left(z_3^{k+1} - z_4^{k+1}\right),
\end{aligned} \tag{27}$$

where ρ_p and ρ_m are the densities of aluminum and Galfenol, respectively, and z_1, z_2, z_3, and z_4 are the z-coordinates at each through-thickness material boundary. The equivalent damping coefficients $\bar{c}_k$ are calculated in a similar manner. The stress resultant N_{xx} is calculated as

$$\begin{aligned}
\textbf{Passive } \mathcal{A}_p : N_{xx} &= \int_{t_{tot}} T_{xx}\, dz = \int_{t_{tot}} \left(C_{11}^{(p)} S_{xx} + C_{12}^{(p)} S_{yy}\right) dz \\
&= \int_{t_{tot}} \left[C_{11}^{(p)}\left(S_{xx}^{(0)} + zS_{xx}^{(1)}\right) + C_{12}^{(p)}\left(S_{yy}^{(0)} + zS_{yy}^{(1)}\right)\right] dz \\
&= \left(C_{11}^{(p)} S_{xx}^{(0)} + C_{12}^{(p)} S_{yy}^{(0)}\right)(z_1 - z_4) \\
&\quad + \frac{1}{2}\left(C_{11}^{(p)} S_{xx}^{(1)} + C_{12}^{(p)} S_{yy}^{(1)}\right)(z_1^2 - z_4^2),
\end{aligned} \tag{28}$$

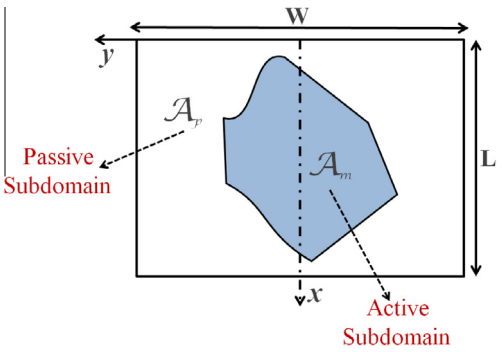

Fig. 2. Equivalent 2-D formulation of the embedded magnetostrictive composite in Fig. 1.

$$\begin{aligned}
\textbf{Active } \mathcal{A}_m : N_{xx} &= \int_{t_{tot}} T_{xx}\, dz = \int_{t_p} T_{xx}\, dz + \int_{t_m} T_{xx}\, dz \\
&= \int_{t_p} \left(C_{11}^{(p)} S_{xx} + C_{12}^{(p)} S_{yy}\right) dz \\
&\quad + \int_{t_m} \left\{C_{11}^{(m)}\left(S_{xx} - \lambda_{xx}\right) + C_{12}^{(m)}\left(S_{yy} - \lambda_{yy}\right)\right\} dz \\
&= \left(C_{11}^{(p)} S_{xx}^{(0)} + C_{12}^{(p)} S_{yy}^{(0)}\right)\left((z_1 - z_2) + (z_3 - z_4)\right) \\
&\quad + \left\{C_{11}^{(m)}\left(S_{xx}^{(0)} - \lambda_{xx}\right) + C_{12}^{(m)}\left(S_{yy}^{(0)} - \lambda_{yy}\right)\right\}(z_2 - z_3) \\
&\quad + \frac{1}{2}\left(C_{11}^{(p)} S_{xx}^{(1)} + C_{12}^{(p)} S_{yy}^{(1)}\right)\left((z_1^2 - z_2^2) + (z_3^2 - z_4^2)\right) \\
&\quad + \frac{1}{2}\left(C_{11}^{(m)} S_{xx}^{(1)} + C_{12}^{(m)} S_{yy}^{(1)}\right)(z_2^2 - z_3^2).
\end{aligned} \tag{29}$$

A similar procedure is applied to calculate the remaining stress resultants. Due to the Galfenol sheet's small thickness, the magnetostrictive strain components λ_{xx}, λ_{yy}, and λ_{xy} are assumed constant through the thickness of each Galfenol layer.

3.5. Computational methodology

The weak form equations are discretized and solved in COMSOL Multiphysics finite element software. The anhysteretic constitutive model for Galfenol is supplied to COMSOL through MATLAB functions to retain the model's full nonlinearity. This work considers cantilever boundary conditions, for which the field-excited composite plate acts as a bending actuator. Thus, the primary output of the model is the tip displacement of the plate.

It has been observed that the 2-D framework has an improved computational efficiency compared to a full 3-D simulation of the same composite structure. The 2-D simulations are approximately *five times faster* than the 3-D framework.

4. Model validation

To validate the model, the tip displacement of a Galfenol–aluminum composite plate was measured in response to quasi-static and dynamic currents produced in an excitation coil. The composite plate (Fig. 4) was manufactured using ultrasonic additive manufacturing (UAM). The welding was performed using a 9 kW Fabrisonic SonicLayer 4000 UAM machine. A single sheet of Galfenol was embedded into the center of the aluminum plate. As shown in Fig. 3, the experimental setup consisted of a magnetic circuit composed of a U-shaped Metglas core upon which the excitation coils were wound, a cantilevering fixture, and the composite plate, which completed the magnetic flux path. The air gap

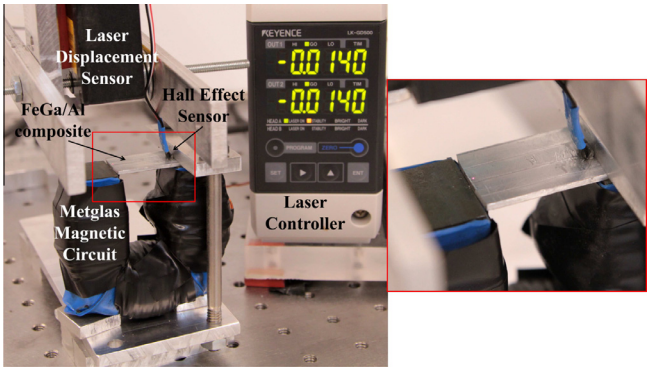

Fig. 3. Experimental setup: cantilevered Galfenol–aluminum composite clamped to U-shaped magnetic circuit made of Metglas; cantilever geometry (also used in validation simulations): $W = 22.9$ mm, $t_{tot} = 1.65$ mm, $b_m = 6.35$ mm, $t_m = 0.965$ mm and $L = 25.1$ mm.

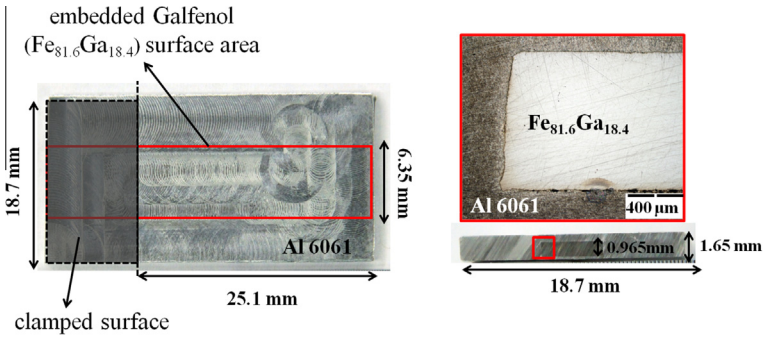

Fig. 4. Geometry of the Galfenol–aluminum composite plate manufactured using ultrasonic additive manufacturing.

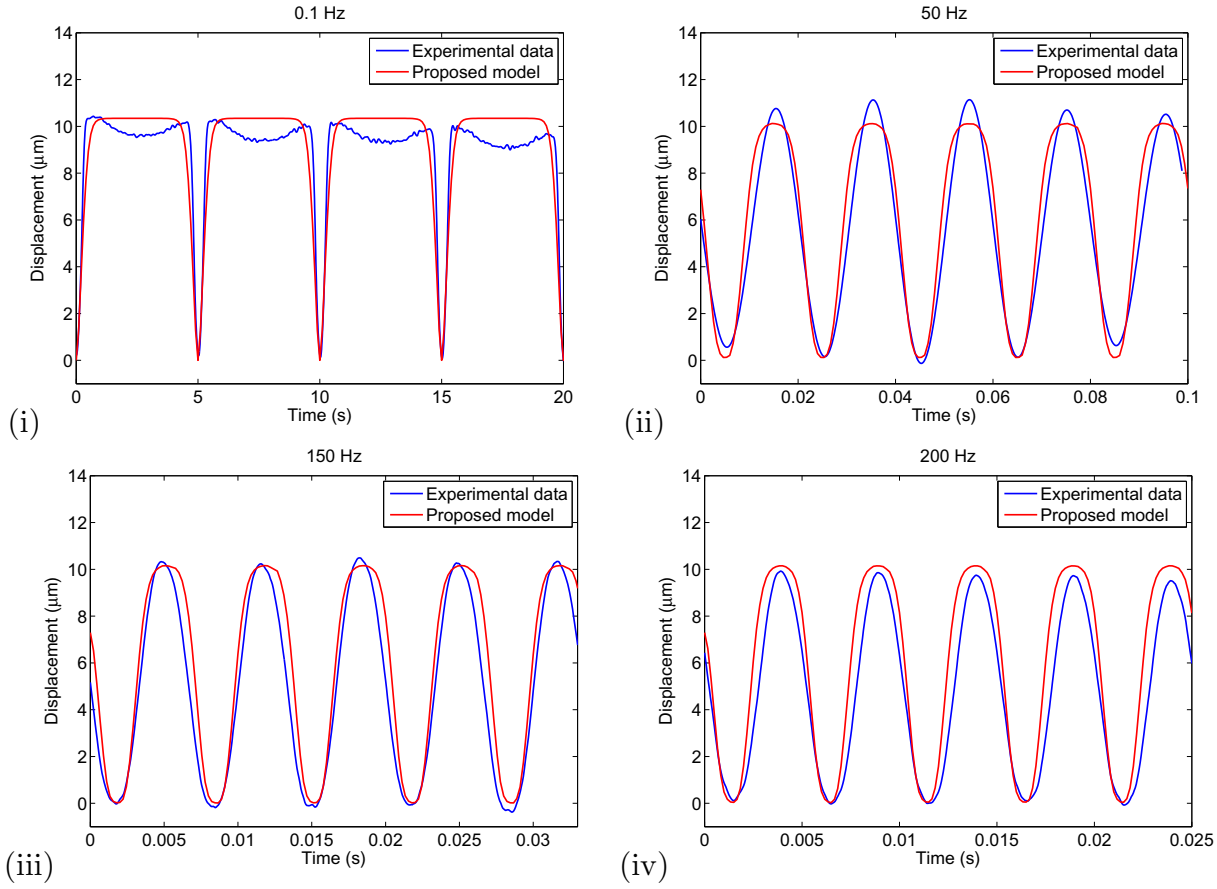

Fig. 5. Comparison of the experimental and simulated dynamic actuation of the Galfenol–aluminum plate at different frequencies: (i) 0.1 Hz, (ii) 50 Hz, (iii) 150 Hz, (iv) 200 Hz.

between the magnetic flux return path and the end of the composite was approximately 0.0254 mm.

The tip displacement of the composite was measured using a Keyence LK-G32 laser displacement sensor having a repeatability of 0.05 micron. A National Instruments cDAQ-9178 was used to acquire data and generate the excitation voltage, which was amplified using a Techron 7782 linear power amplifier. For dynamic tests, sinusoidal excitations of amplitude ≈ 3.25 kA/m were superimposed on a bias field of ≈ 3.50 kA/m, which was used to maximize the magnetic field-induced strain and provide two-way actuation. A comparison between the measured and calculated tip displacement for frequencies up to 200 Hz is shown in Fig. 5. Due to the relatively high stiffness of the plate and low Galfenol volume fraction, the tip displacements are small.

Overall, the model accurately calculates the steady-state, dynamic actuation response of the composite plate up to 200 Hz. However, the model does not capture the transient, wherein a slight decrease in tip displacement is observed as the actuation frequency increases. This can be explained by the lack of electromagnetic dynamics, namely eddy currents, in the model. The inclusion of eddy currents and magnetic field nonuniformity can improve the model's performance.

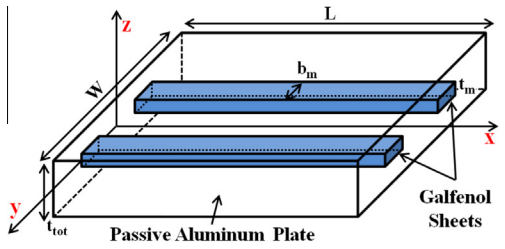

Fig. 6. Galfenol–aluminum composite plate for actuator design study.

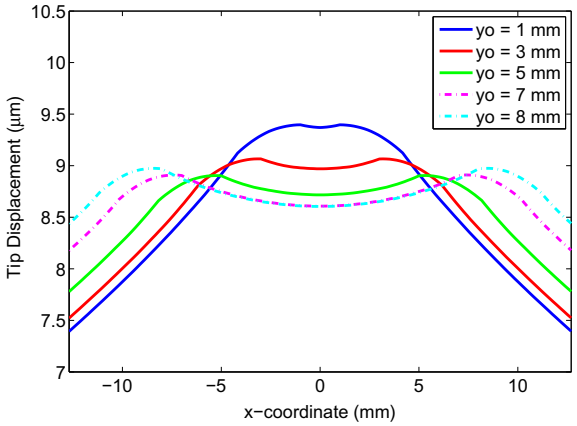

Fig. 7. Variation of tip displacement (μm) along the free end of the composite plate for varying distances (along the *y*-axis) of the Galfenol sheets from the center axis.

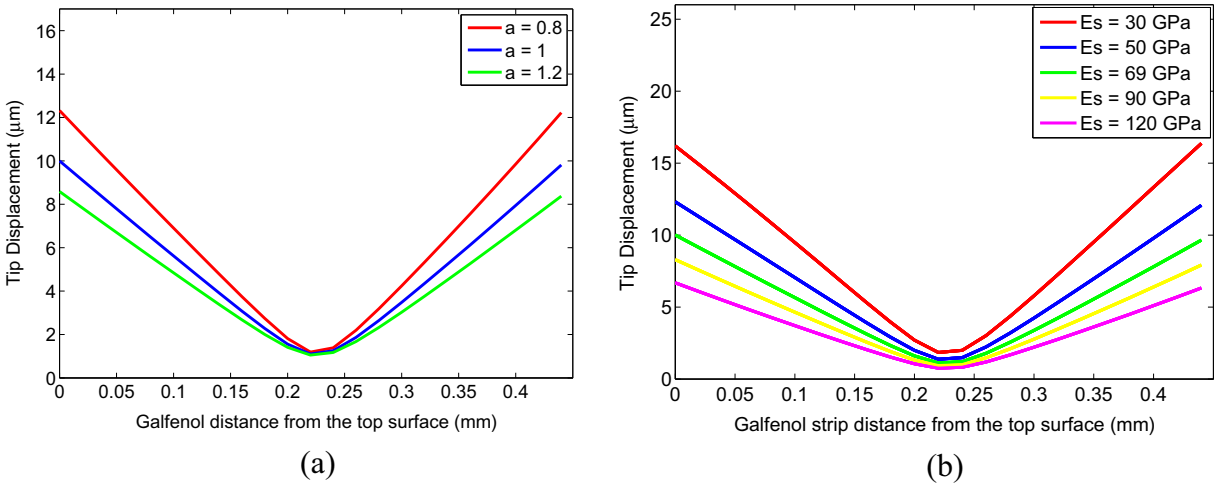

Fig. 8. Variation of tip displacement (μm) as a function of Galfenol sheet's distance from the top surface for different (a) plate aspect ratios (a = width/length), and (b) substrate Young's moduli.

5. Actuator design study: maximizing tip displacements

In this section, we utilize the validated 2-D plate model to maximize the displacements of the Galfenol actuator shown in Fig. 6. Actuator displacements are studied by changing several design parameters while keeping the volume of Galfenol constant.

The actuator is described as follows. The x–y plane of the coordinate system is coincident with the midplane of the composite plate, and the x–z plane is a plane of symmetry. The plate dimensions are: length $L = 25.4$ mm, width $W = 25.4$ mm, and thickness $t_{tot} = 1.45$ mm. The dimensions of each Galfenol patch are: length $L = 25.4$ mm, width $b_m = 3.18$ mm, and thickness $t_m = 0.381$ mm. These sheets are located a distance y_o from the x–z symmetry plane. Finally, the plate is actuated using a conductive coil,[4] which generates sinusoidal and bias magnetic fields that are uniform and oriented along the x-axis.

Using the proposed model, we aim to maximize the composite's tip displacement by modifying: (i) the distance (along y- and z-axes) of the Galfenol sheets from center axis, (ii) the thickness ratio, and (iii) the substrate material properties. Parametric studies are performed by separately varying each of these quantities and, in some cases, for different plate aspect ratios.

[4] The coil and accompanying magnetic circuit need not be modeled due to the assumptions detailed in Section 2.

5.1. Varying Galfenol location along the y-axis

We first study the displacements at the free end of the plate as the Galfenol sheets move away from the x–z axis along the width direction (i.e., as y_o varies). The displacements at every point along the free edge are plotted for five different y_o values in Fig. 7. The results show that the actuator generates highest displacement at the tip's center ($x = L,\ y = 0$) when both of the Galfenol sheets are located at the x–z axis, i.e., when $y_o = 0$. As y_o increases, the displacement at the tip's center decreases and local maxima appear at the x-coordinates about which the Galfenol sheets are centered.

5.2. Varying Galfenol location along the z-axis

Now, the tip displacements of an actuator consisting of a single centered sheet of double the width is considered (i.e., $y_0 = 0$ is fixed). In particular, the tip displacements at $y = 0$ are calculated as the Galfenol layer moves along the thickness (z-axis). The results are plotted for different plate aspect ratios a and substrate moduli Es in Fig. 8. The results demonstrate that the maximum displacement is obtained when the Galfenol sheet is located away from the neutral bending axis. Also, the displacement is more sensitive to changes in aspect ratio and substrate modulus when the Galfenol layer is located away from the neutral axis. The displacement varies linearly with z-coordinate, as assumed in (6)–(8).

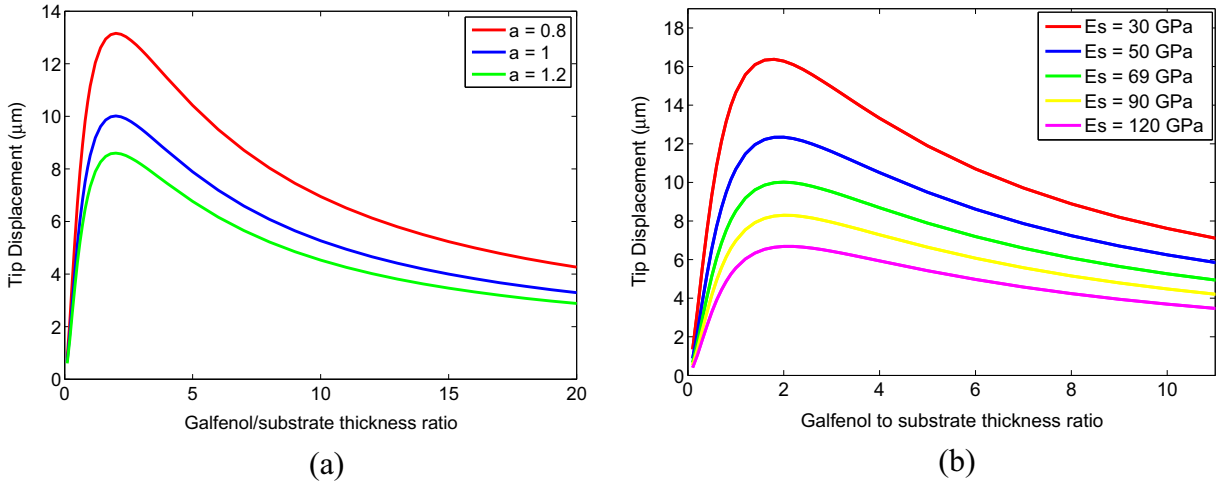

Fig. 9. Variation of tip displacement (μm) as a function of Galfenol/substrate thickness ratio for different (a) plate aspect ratios (a = width/length), and (b) substrate Young's moduli.

5.3. Varying the Galfenol to substrate thickness ratio

According to the results presented in Figs. 7 and 8, the Galfenol layer is fixed at the top of the plate with $y_0 = 0$. The tip displacement is now studied as a function of substrate thickness. The results in Fig. 9 show the existence of a critical thickness ratio beyond which the tip displacements decrease with increasing Galfenol-to-substrate thickness ratio.

The tip displacement is maximized by simultaneously maximizing the Galfenol volume fraction (up to the critical thickness ratio) and the Galfenol sheet's offset from the neutral axis. As the sheet's thickness increases above the critical value, the neutral axis moves within the sheet, thus reducing the bending displacement. Interestingly, a slight increase in the critical thickness ratio is observed with an increase in aspect ratio and substrate modulus. At very high substrate stiffness values, the shape of the curve becomes flatter and the shift in the peak is minimal.

The elastic modulus of the substrate is seen to have a significant impact on the tip displacement. As the substrate's modulus decreases, the flexural rigidity of the beam decreases, thereby providing less resistance to bending deformation for a given magnetostriction-induced force. This result is consistent with the modeling results of Scheidler and Dapino [27], who modeled changes in the stiffness of Galfenol composite beams.

6. Conclusions

A two-dimensional finite element framework for composite plates consisting of magnetostrictive laminae has been developed for transducer applications. The model was developed to accommodate complex geometries, nonlinear magnetostrictive material behavior, and mechanical dynamics. To validate the model and illustrate its usefulness, the model was applied to a prototype bending actuator composed of an aluminum plate with embedded Galfenol sheets. Validation was performed by comparing time-domain tip displacement measurements to simulations for different actuation frequencies.

The nonlinear finite element framework was utilized to perform a design study for a prototype actuator. Parametric studies were performed on key geometric parameters to maximize the actuator's tip displacement. A critical value of the Galfenol/aluminum thickness ratio was observed, above which the tip displacement decreases. It was also observed that the tip displacement increases as the Galfenol sheets move away from the neutral axis. Additionally, the elastic modulus of the substrate had a significant effect on the results of the parametric studies, where a softer modulus resulted in larger displacements.

Acknowledgments

This work was supported by the NASA Aeronautics Scholarship Program (grant # NNX14AE24H). Additional support was provided by the Smart Vehicle Concepts Center (www.SmartVehicleCenter.org), a National Science Foundation Industry/University Cooperative Research Center.

References

[1] Cullity B, Graham C. Introduction to magnetic materials. Wiley.com; 2011.
[2] Atulasimha J, Flatau A. A review of magnetostrictive iron–gallium alloys. Smart Mater Struct 2011;20(4):043001. http://dx.doi.org/10.1088/0964-1726/20/4/043001.
[3] Park G, Bement M, Hartman D, Smith R, Farrar C. The use of active materials for machining processes: a review. Int J Mach Tools Manuf 2007;47(15):2189–206. http://dx.doi.org/10.1016/j.ijmachtools.2007.06.002.
[4] Dapino M. Magnetostrictive materials. Encyclopedia of smart materials. http://dx.doi.org/10.1002/0471216275.esm051.
[5] Wun-Fogle M, Savage H, Clark A. Sensitive, wide frequency range magnetostrictive strain gage. Sens Actuators 1987;12(4):323–31. http://dx.doi.org/10.1016/0250-6874(87)80052-5.
[6] Bitar S, Probst J, Garshelis I. Development of a magnetoelastic torque sensor for formula 1 and champ car racing applications. SAE Trans 2000;109(7):42–9. http://dx.doi.org/10.4271/2000-01-0085.
[7] Guntupalli R, Lakshmanan R, Hu J, Huang T, Barbaree J, Vodyanoy V, et al. Rapid and sensitive magnetoelastic biosensors for the detection of salmonella typhimurium in a mixed microbial population. J Microbiol Methods 2007;70(1):112–8. http://dx.doi.org/10.1016/j.mimet.2007.04.001.
[8] Basantkumar R, Stadler B, Robbins W, Summers E. Integration of thin-film galfenol with mems cantilevers for magnetic actuation. IEEE Trans Magn 2006;42(10):3102–4. http://dx.doi.org/10.1109/TMAG.2006.879666.
[9] Friel R, Harris R. Ultrasonic additive manufacturing – a hybrid production process for novel functional products. Procedia CIRP 2013;6:35–40. http://dx.doi.org/10.1016/j.procir.2013.03.004.
[10] Yang Y, Stucker B, Ram G. Mechanical properties and microstructures of SiC fiber-reinforced metal matrix composites made using ultrasonic consolidation. J Compos Mater 2010;44(26):3179–94. http://dx.doi.org/10.1177/0021998310371528.
[11] Hahnlen R, Dapino M. Performance and modeling of active metal-matrix composites manufactured by ultrasonic additive manufacturing. In: SPIE smart structures and materials + nondestructive evaluation and health monitoring, international society for optics and photonics; 2011. p. 797903. http://dx.doi.org/10.1117/12.881152.
[12] Mindlin R. High frequency vibrations of piezoelectric crystal plates. Int J Solids Struct 1972;8(7):895–906. http://dx.doi.org/10.1016/0020-7683(72)90004-2.

[13] Bechtel S, Cao J, Forest M. Practical application of a higher order perturbation theory for slender viscoelastic jets and fibers. J Non-Newtonian Fluid Mech 1992;41(3):201–73. http://dx.doi.org/10.1016/0377-0257(92)87001-R.
[14] Reddy J. On laminated composite plates with integrated sensors and actuators. Eng Struct 1999;21(7):568–93. http://dx.doi.org/10.1016/S0141-0296(97)00212-5.
[15] Kannan K, Dasgupta A. A nonlinear Galerkin finite-element theory for modeling magnetostrictive smart structures. Smart Mater Struct 1997;6(3):341. http://dx.doi.org/10.1088/0964-1726/6/3/011.
[16] Datta S, Atulasimha J, Mudivarthi C, Flatau A. Modeling of magnetomechanical actuators in laminated structures. J Intell Mater Syst Struct 2009;20(9):1121–35. http://dx.doi.org/10.1177/1045389X09104262.
[17] Datta S, Atulasimha J, Mudivarthi C, Flatau A. The modeling of magnetomechanical sensors in laminated structures. Smart Mater Struct 2008;17(2):025010. http://dx.doi.org/10.1088/0964-1726/17/2/025010.
[18] Shu L, Headings L, Dapino M, Chen D, Lu Q. Nonlinear model for galfenol cantilevered unimorphs considering full magnetoelastic coupling. J Intell Mater Syst Struct http://dx.doi.org/10.1177/1045389X13489600.
[19] Evans P, Dapino M. Efficient magnetic hysteresis model for field and stress application in magnetostrictive galfenol. J Appl Phys 2010;107(6):063906–063906-11. http://dx.doi.org/10.1063/1.3318494.
[20] Reddy J. Mechanics of laminated composite plates and shells: theory and analysis. CRC; 2003.
[21] Chakrabarti S, Dapino M. Nonlinear finite element model for 3D Galfenol systems. Smart Mater Struct 2011;20(10):105034. http://dx.doi.org/10.1088/0964-1726/20/10/105034.
[22] Evans P, Dapino M. Dynamic model for 3-D magnetostrictive transducers. IEEE Trans Magn 2011;47(1):221–30. http://dx.doi.org/10.1109/TMAG.2010.2088130.
[23] Weng L, Walker T, Deng Z, Dapino M, Wang B. Major and minor stress-magnetization loops in textured polycrystalline $Fe_{81.6}Ga_{18.4}$ galfenol. J Appl Phys 2013;113(2):024508. http://dx.doi.org/10.1063/1.4772722.
[24] Chakrabarti S, Dapino M. Fully coupled discrete energy-averaged model for Terfenol-D. J Appl Phys 2012;111(5):054505. http://dx.doi.org/10.1063/1.3687372.
[25] Armstrong W. An incremental theory of magneto-elastic hysteresis in pseudo-cubic ferro-magnetostrictive alloys. J Magn Magn Mater 2003;263:208–18. http://dx.doi.org/10.1016/S0304-8853(02)01567-6.
[26] Chakrabarti S. Modeling of 3D magnetostrictive systems with application to galfenol and terfenol-D transducers [Ph.D. thesis]. The Ohio State University; 2011.
[27] Scheidler JJ, Dapino MJ. Stiffness tuning of FeGa structures manufactured by ultrasonic additive manufacturing. In: Proceedings of SPIE, vol. 9059; 2014. p. 905907. http://dx.doi.org/10.1117/12.2046247.